Hindawi
Journal of Chemistry
Volume 2019, Article ID 3428681, 8 pages
https://doi.org/10.1155/2019/3428681

Research Article

A Facile Synthesis, Characterization, and Photocatalytic Activity of Magnesium Ferrite Nanoparticles via the Solution Combustion Method

Loan T. T. Nguyen,[1] **Lan T. H. Nguyen**,[1] **Nhuong Chu Manh**,[1] **Dung Nguyen Quoc**,[1] **Hai Nguyen Quang**,[2] **Hang T. T. Nguyen**,[3] **Duy Chinh Nguyen**,[4] **and Long Giang Bach**[4,5]

[1]*Faculty of Chemistry, Thai Nguyen University of Education, Thai Nguyen University, Thai Nguyen, Vietnam*
[2]*Faculty of Physics, Thai Nguyen University of Education, Thai Nguyen University, Thai Nguyen, Vietnam*
[3]*Thai Nguyen University of Technology, Thai Nguyen University, Thai Nguyen, Vietnam*
[4]*NTT Hi-Tech Institute, Nguyen Tat Thanh University, Ho Chi Minh City, Vietnam*
[5]*Faculty of Chemical Engineering and Food Technology, Nguyen Tat Thanh University, Ho Chi Minh City, Vietnam*

Correspondence should be addressed to Loan T. T. Nguyen; nguyentoloan@dhsptn.edu.vn

Received 27 November 2018; Revised 23 January 2019; Accepted 3 March 2019; Published 25 March 2019

Academic Editor: Darren Sun

In this study, we adopted the solution combustion method to synthesize magnesium ferrite ($MgFe_2O_4$) using urea as the fuel. Various techniques including TGA, XRD, SEM, TEM, FTIR, UV-Vis DRS, and EDS were employed to characterize the synthesized $MgFe_2O_4$ nanoparticles. The XRD analysis revealed that single-phase $MgFe_2O_4$ was formed at a calcination temperature of at 500–600°C for 3 hours in the absence of an intermediate phase. TEM analysis also revealed the formation of monodisperse magnesium ferrite nanoparticles, averaged at 30 nm in size. The photocatalytic activity of the synthesized $MgFe_2O_4$ nanoparticles against methylene blue dye under visible light was investigated, showing the efficiency of 89.73% after 240 minutes of light irradiation with the presence of H_2O_2.

1. Introduction

Ferrite nanoparticles, MFe_2O_4 where M is any divalent metal ions such as Mg, Mn, Ni, Co, Fe, Cu, etc, find wide applications in several fields [1]. Depending on the area of application, ferrite nanoparticles need to exhibit distinct characteristics. For example, in order to be suitable as an absorbent for decontamination of wastewater, ferrites should have exceptional chemical reactivity, adsorption capacity, and most importantly, reasonable M_s value, which is critical for magnetic recovery of the adsorbent from the aqueous solution [2]. The choice of synthesis method should also be considered when it comes to exploring the mechanism of formation of ferrite properties. To be specific, the distribution of metallic ions among crystallographic lattice sites, which defines the characteristics of the materials, largely depends on the synthesis method. This effectively makes the method selection crucial when it comes to adapting the materials to the needs of application [1, 3, 4].

Usually, the maximum band gap energy of ferrites is approximately 2 eV, allowing the materials to effectively absorb visible light [5]. Furthermore, advantageous magnetic properties also offer ferrites useful applications [6]. Both forms of ferrites, in individual photocatalysts or in combination with others, are accentuated in literature for being separable and reusable from the reaction mixture [5, 7]. One of the typical uses of ferrites is as visible light photocatalysts for the degradation of pollutants in water and wastewater [7–10]. This capability of ferrite catalysts is

possible due to effective utilization of light energy, which in turn allows formation of e^-/h^+ pairs on the photocatalytic surface. The e^-/h^+ pairs, owing to their susceptibility to oxidation and reduction, play an important role in formation of reactive oxygen species, such as $^\bullet OH$ and $O_2^{\bullet-}$, consequently promoting the decomposition of pollutants. Previous studies also suggested the addition of oxidants such as H_2O_2 into the reaction to create a Fenton-type system [6, 8, 11, 12] aiding the degradation through formation of hydroxyl radicals.

Among magnetic ferrites, magnesium ferrite ($MgFe_2O_4$) is a typical inverse spinel, where Fe^{3+} ions are located in the tetrahedral (A) and octahedral (B) sites and Mg^{2+} ions are located in octahedral sites only [13]. The application of magnesium ferrite is diverse ranging from that in high-density recording media [14] to that in the fields of heterogeneous catalysis [7, 15–17], adsorption [18–20], anode material [21], cancer cure [22], and sensors [23]. In addition, the material is also a soft magnetic n-type semiconducting materials with a narrow band gap (1.9 eV) [24].

Methods devised for preparation of magnesium ferrite nanocrystallites included the coprecipitation method [19, 25–28], sol-gel method [20, 29], combustion method [30, 31], hydrothermal method [32], thermal decomposition method [33], and solvothermal method [34]. Among the methods used to synthesize ferrite nanoparticles, the solution combustion synthesis is favored for its simplicity, short reaction time, and low annealing temperature [35]. These advantages have made resulting ferrites to have fine particle size, reduced impurities, and improved physical properties [36]. In the combustion reaction, the fuels play the role of forming complexes with metal cations [35]. Frequently used fuels in previous studies included glycine, urea, citric acid, and EDTA (ethylene diammin tetraacetic acid). In this work, $MgFe_2O_4$ nanoparticles are prepared by the solution combustion method with urea as fuel. The structural, chemical composition, thermal, morphology, and photocatalytic activity of $MgFe_2O_4$ nanoparticles are investigated.

2. Materials and Method

2.1. Materials. All chemicals including magnesium nitrate hexahydrate ($Mg(NO_3)_2{\cdot}6H_2O$), iron nitrate nonahydrate ($Fe(NO_3)_3{\cdot}9H_2O$), urea (CH_4N_2O), and methylene blue ($C_{16}H_{18}ClN_3S$) were obtained from Merck and used as received.

2.2. Preparation of $MgFe_2O_4$ Nanoparticles. The combustion preparation of $MgFe_2O_4$ with urea fuel in this study is described as follows. First, urea was dissolved in water, followed by an appropriate amount of magnesium nitrate hexahydrate and iron nitrate nonahydrate following the mole ratio for Mg(II)/Fe(III) of 1 : 2 under vigorous stirring to form a mixed solution. Afterwards, the mixed solution was further stirred for 4 hours until gel was formed. The gel was then dried in an oven at 80°C for 10 hours. Finally, the precipitate was calcined at 500–800°C for 3 hours with a heating rate of 5°C·min^{-1} [37].

2.3. Characterizations. The gel precursor was studied for its thermal decomposition behavior through thermogravimetry (TG) and differential thermal analysis (DTA) on a Labsys Evo S60/58988 instrument (Setaram, France) in the temperature range of 30–800°C with the heating rate of 10°C·min^{-1}. The phase of the obtained powder was characterized by X-ray diffraction (XRD) using a D8 Advance diffractometer (Bruker, Madison, WI, USA) with CuK_α radiation ($\lambda = 1.5406$ Å) in a 2θ angle ranging from 20° to 70° with a step of 0.03°. The crystallite size of spinel (D) was determined by Scherrer formula:

$$D = \frac{k\lambda}{\beta \cos\theta}, \quad (1)$$

where λ, k, β, and θ are the X-ray wavelength (0.1504 nm), Scherrer constant (0.89), the full width at half maximum measured in radians, and the angle of diffraction of the (311) peak with the highest intensity, respectively. The morphological properties were analyzed by two techniques including scanning electron microscopy (SEM, Hitachi S-4800, Japan) and transmission electron microscopy (TEM, JEOL-JEM-1010, Japan). For sample composition, energy dispersive X-ray spectroscopy (EDX, JEOL JED 2300 Analysis Station, Japan) was employed. The spinel structure is confirmed for formation by Fourier transform infrared spectroscopy (FTIR Affinity-1S, Shimadzu, Japan). The optical absorption spectra were recorded by UV-Vis absorption spectrometer (U-4100, Hitachi, Japan).

2.4. Photocatalytic Degradation of Methylene Blue. The conditions in which experiments are conducted include room temperature, pH of approximately 7 for methylene blue (MB), and continuous circulation mode. Prior to the photocatalytic reaction, the adsorption/desorption equilibrium of the aqueous solution containing the suspension was achieved by stirring in dark environment for 30 mins. 50 mg of $MgFe_2O_4$ was dispersed into 100 mL of MB aqueous solution (10 mg·L^{-1}). Subsequently, H_2O_2 was introduced and irradiation on the suspension followed immediately using 40 W Compact lamps, Philips. The photocatalytic efficiency of MB (H) was calculated using the following equation:

$$H = \frac{C_0 - C_t}{C_0} \times 100\%, \quad (2)$$

where C_0 is the concentration of MB (mg·L^{-1}). The subscripts 0 and t denote time points where concentration was measured, at initial equilibrium (0) and after t irradiation time, respectively. Concentration was measured by an ultraviolet-visible spectrophotometer (UV-1700 Shimadzu, Japan) with a wavelength of 664 nm.

3. Results and Discussion

3.1. Structural Characterization. In the precursor, urea is not only to provide sufficient heat for the system but also to ensure the formation of stable complexes with the metal ions to increase their solubility and prevent selective precipitation of

metal ions during water removal. The reaction for metal nitrate mixture using urea as the fuel assuming complete combustion may be represented by the following equation [38]:

$$3Mg(NO_3)_2 + 6Fe(NO_3)_3 + 20CH_4N_2O \longrightarrow 3MgFe_2O_4 + 20CO_2 + 32N_2 + 40H_2O \quad (3)$$

The TG/DTA of the ferrite precursor are shown in Figure 1(a). It can be observed that there are two exothermal peaks at 137.86°C and 437.04°C. The exothermal peak at 137.86°C has suggested self-combustion, like a process in which the nitrate ions act as an oxidizing agent and urea as fuel. The maximum exothermal peak at 437.04°C could be observed to closely follow a substantial mass loss in the temperature range of 200–450°C, evidencing the occurrence of the decomposition reaction of the ferrite precursor and nitrate. Approximately, the total mass loss that precedes the sharp exothermal reaction is 81.04%, which is consistent with the theoretical result (80.31%). This could be attributable to the relief of gases CO_2, H_2O, and N_2 from the precursor. At temperature higher than 450°C, the weight of the sample remained almost constant. Therefore, the calcining temperature of the samples was selected in the range from 500 to 800°C.

Figure 1(b) displays the FTIR spectra of the $MgFe_2O_4$ precursor and two calcined samples at 500 and 600°C relative to the range of 4000–400 cm^{-1}. For the precursor sample, three broad absorption bands were observed at approximately 3446, 1656, and 1384 cm^{-1}, respectively, corresponding to the presence of hydroxyl groups (-OH), the stretching vibration of the carboxyl group, and the presence of NO_3^- ions [29]. In the two spectra of the $MgFe_2O_4$ calcined at 500–600°C, two bands at 582 and 586 cm^{-1} and two bands at 443 and 445 cm^{-1} could be pairwise indexed to the stretching vibrations of metal-oxygen bonds in tetrahedron sites and in octahedron sites, respectively, suggesting the formation of magnesium ferrite [15, 20]. In addition, the absorption broad bands at 3450 and 3425 cm^{-1} are, respectively, indicative of the stretching mode of H_2O molecules and hydroxyl groups, and in turn, the presence of H_2O molecules on the surface of $MgFe_2O_4$ nanoparticles [24].

Figure 2 displays different X-ray diffraction patterns of $MgFe_2O_4$ nanoparticles with temperature varying from 500 to 800°C. The two ferrite samples calcined at 500–600°C were obtained as single spinel phase with peaks at 220, 311, 400, 511, and 440, corresponding to the cubic spinel structure (JCPDS card. no. 01-071-1232) [26]. It is showed that the increase in temperature is associated with the improvement of $MgFe_2O_4$ powders. However, from 700 to 800°C, new phases of α-Fe_2O_3 were observed. The spinel phase of $MgFe_2O_4$ was confirmed by five XRD peaks at 220, 311, 400, 511, and 440 crystal planes. Results reported in Table 1 also indicate that the crystallite size of $MgFe_2O_4$ was positively associated with the calcination temperature. As temperature moved from 500 to 800°C with 100°C interval, the average crystallite size was expanded from 18 to 61 nm. For the "a" lattice parameter, XRD spectra showed that for $MgFe_2O_4$ nanoparticles, the value fell in the range of 8.344–8.378 Å.

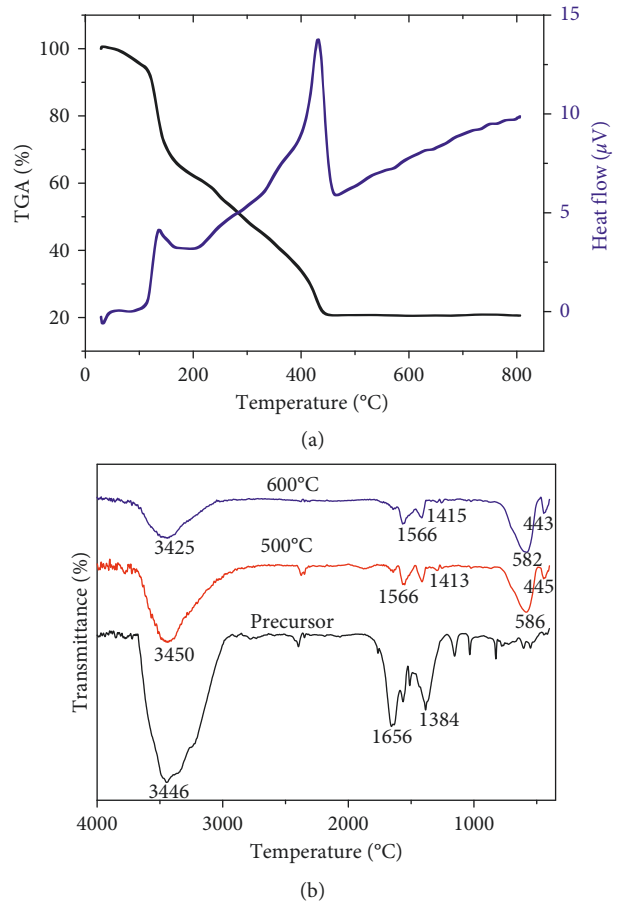

Figure 1: TGA/DTA curve of the precursor (a) and FT-IR spectra of the precursor and $MgFe_2O_4$ calcined samples at 500–600°C (b).

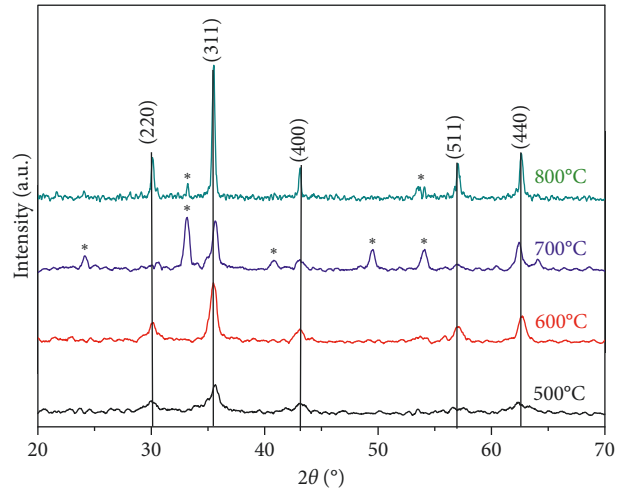

Figure 2: X-ray diffraction of $MgFe_2O_4$ calcined samples from 500°C to 800°C.

The SEM images of different samples of $MgFe_2O_4$ nanoparticles corresponding to four calcination temperature points of 500°C, 600°C, 700°C, and 800°C are shown in Figures 3(a)–3(d). Visually, the images showed consistent implication with the XRD results. To be specific,

Table 1: Average crystallite size, lattice parameter, and unit cell volume of the samples at different calcination temperatures.

t_c (°C)	Average crystallite size (nm)	Lattice constant a (Å)	Cell volume V (Å^3)
500	18	8.348	581.76
600	24	8.378	588.06
700	28	8.344	581.06
800	61	8.367	585.75

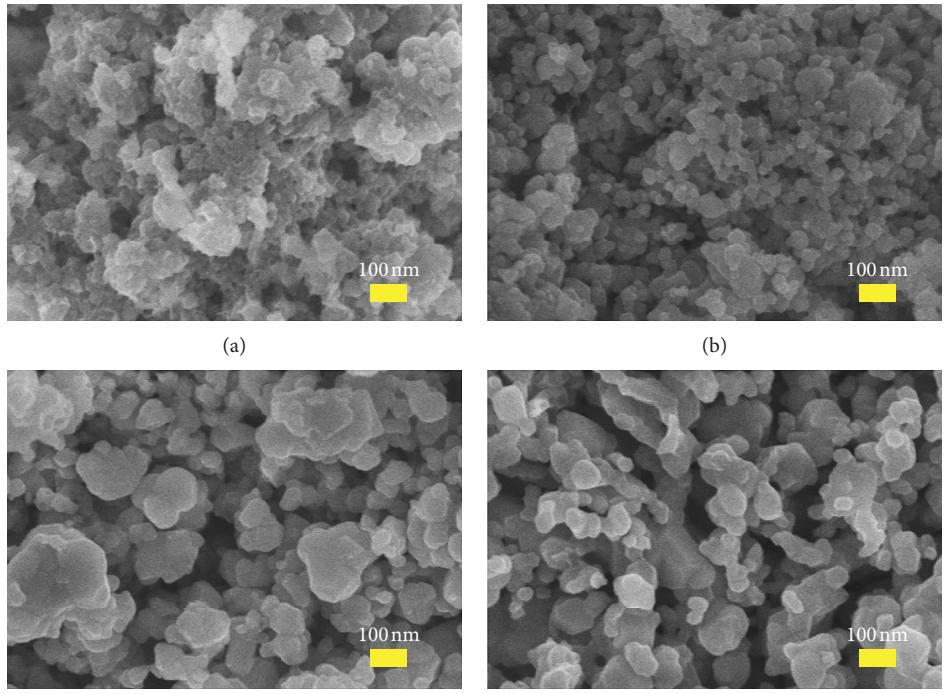

Figure 3: SEM of $MgFe_2O_4$ calcined samples at 500°C (a), 600°C (b), 700°C (c), and 800°C (d).

particle size of the prepared samples were found to be proportionally increasing with temperature. This could possibly be due to the aggregation and coalescence during desiccation.

The TEM image of $MgFe_2O_4$ synthesized at 500°C is presented in Figure 4(a). Evidently, the magnesium ferrite nanoparticles resulted from the solution combustion method were uniform in terms of morphology and crystallite size and reached the particle size of approximately 30 nm.

Figure 4(b) shows chemical purities and elemental composition of the $MgFe_2O_4$ materials produced by energy dispersive X-ray analysis (EDX). The existence of Mg, O, and Fe was determined by their corresponding peaks and the absence of other characteristic peaks. On the contrary, the synthesized sample was pure and did not contain any other elements.

The UV-Visible absorption spectrum was obtained to investigate the optical properties of magnesium ferrite calcined at 500–600°C as shown in Figure 5. By using the Kubelka–Munk equation, the band gap of $MgFe_2O_4$ samples was determined from reflectance spectra via conversion to absorbance [39]. The band gap energy E_g (eV) of the synthesized photocatalyst is calculated by the following equation:

$$E_g = \frac{h \cdot c}{\lambda_{max}} = \frac{1240}{\lambda_{max}}, \quad (4)$$

where h, c, and λ_{max} are the Planck constant ($6.62.10^{-34}$ J·s·photon^{-1}), the speed of light (3.10^{-8} m·s^{-1}), and the wavelength at the absorption edge (nm), respectively [40]. At wavelengths 500 and 600°C, λ_{max} of the samples was calculated to be 679 nm and 687 nm, respectively. Therefore, the calculated band gap energy values are 1.83 eV and 1.81 eV for the $MgFe_2O_4$ samples calcined at 500°C and 600°C, respectively.

3.2. Photocatalytic Activity of Magnesium Ferrite Nanoparticles. Nanoparticles of the $MgFe_2O_4$ were tested for catalytic activities by performing photo-Fenton-like degradation of MB. Figures 6(a)–6(e) show different UV-Visible spectra of MB with $MgFe_2O_4$ photocatalyst corresponding to varying conditions including the calcination temperature of the absorbent, availability of H_2O_2, and presence of light irradiation.

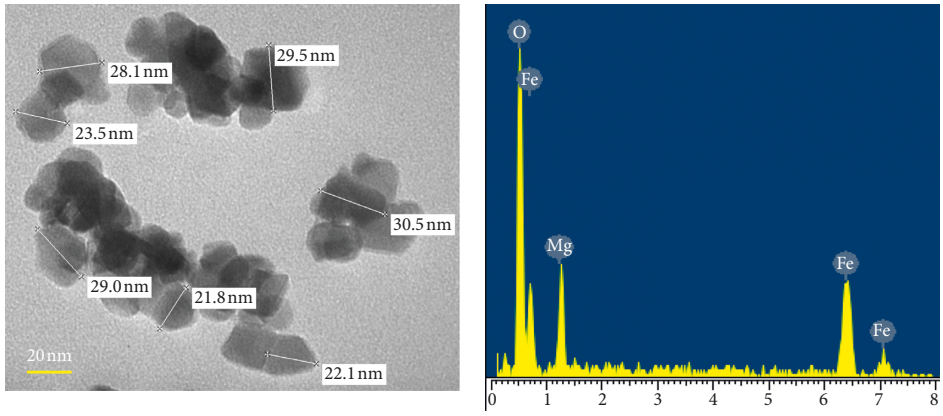

(a) (b)

Figure 4: TEM and EDS of $MgFe_2O_4$ calcined sample at 500°C.

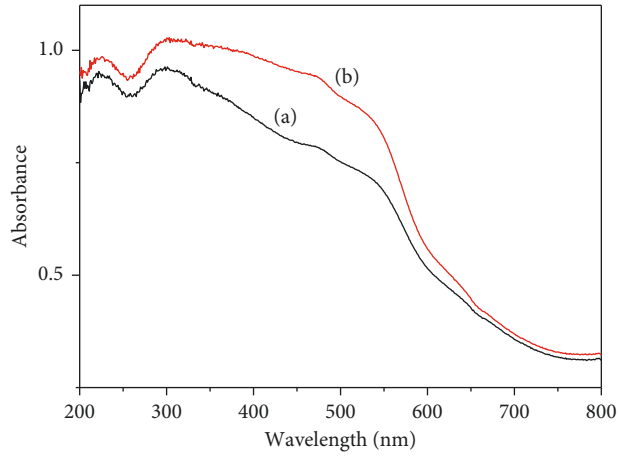

Figure 5: The UV-Vis diffuse reflectance spectra of $MgFe_2O_4$ calcined at 500–600°C.

The presence of methylene blue is indicated by the two absorption peaks at 609 nm and 664 nm [7]. It is visibly observed that the color of the MB solution gradually changed from blue to light blue and finally to colorless, which is presumably due to the estrangement of the chromophoric group. In the first two spectra where H_2O_2 was absent, MB degradation efficiency reached 6.51% (in the dark) and 31.73% (under light irradiation) after 240 minutes, suggesting the positive influence of light on the degradation efficiency. In comparison with the first spectrum, the third spectrum involved the introduction of H_2O_2, showing a significantly higher efficiency at 35.48%. The last two spectra demonstrated the effect of calcination temperature with the presence of H_2O_2 and light irradiation. The measured efficiencies were 89.73% and 69.17% corresponding to $MgFe_2O_4$ calcined at 500°C and 600°C, respectively. In addition, significant and proportional decline of peak intensity with respect to irradiation time was also recognized in these two spectra. These results suggested that light irradiation, ferrite catalyst, and H_2O_2 were all required for efficient photo-Fenton degradation of MB dye. Similar results have been reported for $NiFe_2O_4$ nanoparticles and $CuFe_2O_4$ spheres by various studies [11, 41].

Thus, it is possible to affirm that the main factors for the photodegradation of methylene blue are the crystallite size and the surface area of the $MgFe_2O_4$ nanoparticles. The particle size of the calcined sample at 500°C is smaller than that of the calcined sample at 600°C. Therefore, the photocatalytic activity of the sample at 500°C is higher than that of the calcined sample at 600°C. This effect was also observed in the case of the methylene blue degradation in the presence of the copper ferrite nanopowders [42] and in the presence of coating titania-silica on cobalt ferrite nanoparticles [43].

A pseudo-first-order kinetic model was adopted to describe the degradation process in the heterogeneous Fenton/photo-Fenton catalysis system [11, 44, 45]. Figure 6(f) plots $\ln(C_o/C_t)$ versus irradiation time (t) for the $MgFe_2O_4$ sample, showing an approximated linear relationship between the two variables. This indicates that the photodegradation of MB follows a pseudo-first-order reaction. Calculation of linear slopes revealed that the rate constant

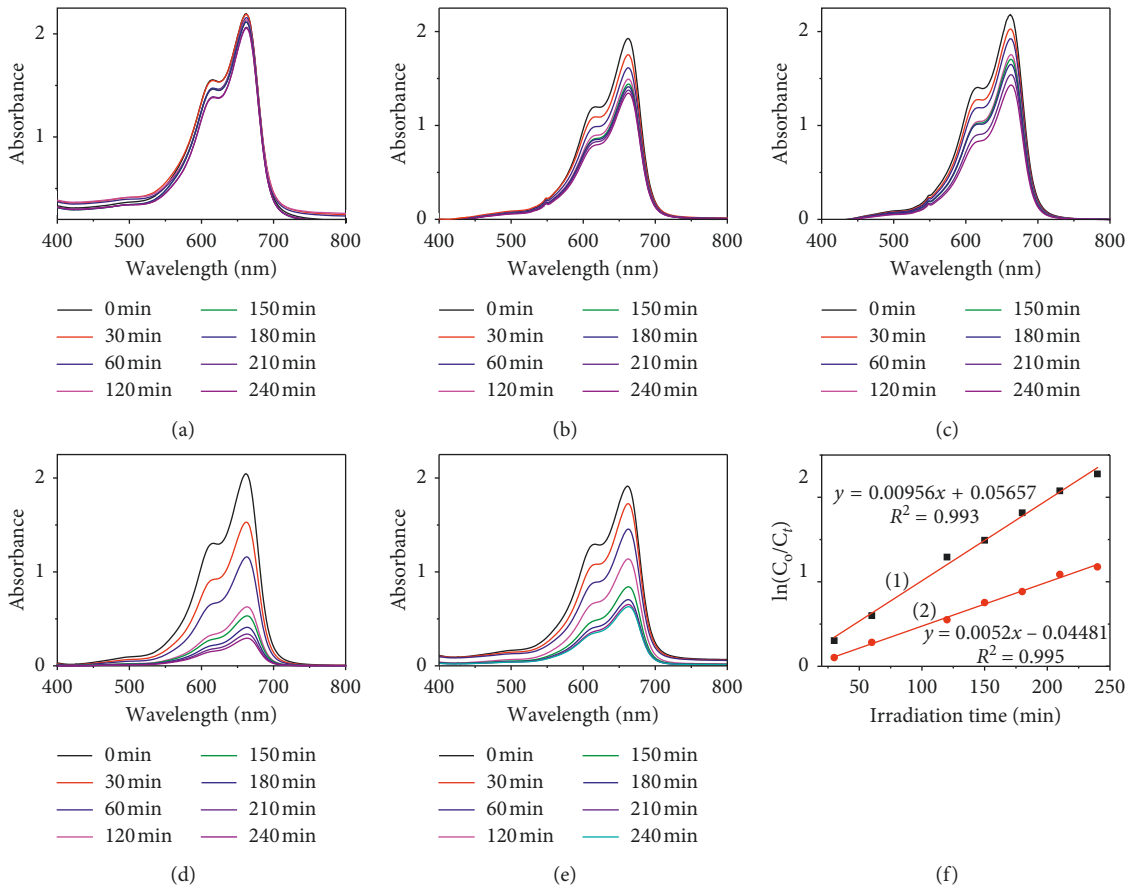

Figure 6: UV-Visible spectra of MB in different conditions and calcination temperatures of $MgFe_2O_4$ catalyst: (a) 500°C + dark, (b) 500°C + light, (c) 500°C + H_2O_2 + dark, (d) 500°C + H_2O_2 + light, (e) 600°C + H_2O_2 + light, and (f) the plots of ln (C_o/C_t) versus irradiation time (t) in the presence of $MgFe_2O_4$ calcined samples at 500°C (1) and 600°C (2).

(k) for the $MgFe_2O_4$ samples calcined at 500°C and 600°C were 0.00956 min^{-1} and 0.0052 min^{-1}, respectively.

4. Conclusions

We have successfully synthesized $MgFe_2O_4$ nanoparticles using the solution combustion method with urea as fuel. The particle size of prepared samples was showed to be proportional with rising temperature. Phase-pure $MgFe_2O_4$ nanoparticles were obtained at 500–600°C for 3 h with the size about 30 nm. UV-Vis also approximated the band gap which ranged from 1.81 to 1.83 eV. The present study also highlighted the role of $MgFe_2O_4$ in the degradation (89.73% in 240 minutes) of MB dye, suggesting possible applications of the ferrite for photo-Fenton activity in decontamination of wastewater. Kinetics describing the photodegradation process of two samples calcined at 500°C and 600°C also revealed that the reaction adhered to pseudo-first order with a rate constant (k) of 0.00956 min^{-1} and 0.0052 min^{-1}, respectively.

Data Availability

The data used to support the findings of this study are available from the corresponding author upon request.

Conflicts of Interest

The authors declare that they have no conflicts of interest.

References

[1] Z. Cao, J. Zhang, J. Zhou et al., "Electroplating sludge derived zinc-ferrite catalyst for the efficient photo-Fenton degradation of dye," *Journal of Environmental Management*, vol. 193, pp. 146–153, 2017.

[2] K. K. Kefeni, B. B. Mamba, and T. A. M. Msagati, "Application of spinel ferrite nanoparticles in water and wastewater treatment: a review," *Separation and Purification Technology*, vol. 188, pp. 399–422, 2017.

[3] B. Pourgolmohammad, S. M. Masoudpanah, and M. R. Aboutalebi, "Synthesis of $CoFe_2O_4$ powders with high surface area by solution combustion method: effect of fuel content and cobalt precursor," *Ceramics International*, vol. 43, no. 4, pp. 3797–3803, 2017.

[4] S. I. Hussein, A. S. Elkady, M. M. Rashad, A. G. Mostafa, and R. M. Megahid, "Structural and magnetic properties of magnesium ferrite nanoparticles prepared via EDTA-based sol-gel reaction," *Journal of Magnetism and Magnetic Materials*, vol. 379, pp. 9–15, 2015.

[5] E. Casbeer, V. K. Sharma, and X. Z. Li, "Synthesis and photocatalytic activity of ferrites under visible light: a review," *Separation and Purification Technology*, vol. 87, pp. 1–14, 2012.

[6] P. A. Vinosha, B. Xavier, D. Anceila, and S. J. Das, "Nanocrystalline ferrite (MFe_2O_4, M = Ni, Cu, Mn and Sr) photocatalysts synthesized by homogeneous Co-precipitation technique," *Optik*, vol. 157, pp. 441–448, 2018.

[7] M. Shahid, L. Jingling, Z. Ali et al., "Photocatalytic degradation of methylene blue on magnetically separable $MgFe_2O_4$ under visible light irradiation," *Materials Chemistry and Physics*, vol. 139, no. 2-3, pp. 566–571, 2013.

[8] M. Sundararajan, L. John Kennedy, P. Nithya, J. Judith Vijaya, and M. Bououdina, "Visible light driven photocatalytic degradation of rhodamine B using Mg doped cobalt ferrite spinel nanoparticles synthesized by microwave combustion method," *Journal of Physics and Chemistry of Solids*, vol. 108, pp. 61–75, 2017.

[9] S. K. Rashmi, H. S. Bhojya Naik, H. Jayadevappa, R. Viswanath, S. B. Patil, and M. Madhukara Naik, "Solar light responsive Sm-Zn ferrite nanoparticle as efficient photocatalyst," *Materials Science and Engineering: B*, vol. 225, pp. 86–97, 2017.

[10] E. Aghabeikzadeh-Naeini, M. Movahedi, N. Rasouli, and Z. Sadeghi, "Synthesis of $ZnFe_2O_4$ nanoparticles in presence and absence of tween-20: optical property, adsorption and photocatalytic activity," *Materials Science in Semiconductor Processing*, vol. 73, pp. 72–77, 2018.

[11] X. Guo, K. Wang, D. Li, and J. Qin, "Heterogeneous photo-Fenton processes using graphite carbon coating hollow $CuFe_2O_4$ spheres for the degradation of methylene blue," *Applied Surface Science*, vol. 420, pp. 792–801, 2017.

[12] S. Q. Liu, L. R. Feng, N. Xu, Z. G. Chen, and X. M. Wang, "Magnetic nickel ferrite as a heterogeneous photo-Fenton catalyst for the degradation of rhodamine B in the presence of oxalic acid," *Chemical Engineering Journal*, vol. 203, pp. 432–439, 2012.

[13] I. Khishigdemberel, E. Uyanga, H. Hirazawa, and D. Sangaa, "Influence of Cu dope on the structural behavior of $MgFe_2O_4$ at various temperatures," *Physica B: Condensed Matter*, vol. 544, pp. 73–78, 2018.

[14] Y. Huang, Y. Tang, J. Wang, and Q. Chen, "Synthesis of $MgFe_2O_4$ nanocrystallites under mild conditions," *Materials Chemistry and Physics*, vol. 97, no. 2-3, pp. 394–397, 2006.

[15] H. Zhou, L. Hu, J. Wan et al., "Microwave-enhanced catalytic degradation of p-nitrophenol in soil using $MgFe_2O_4$," *Chemical Engineering Journal*, vol. 284, pp. 54–60, 2016.

[16] C. J. Jia, Y. Liu, M. Schwickardi et al., "Small gold particles supported on $MgFe_2O_4$ nanocrystals as novel catalyst for CO oxidation," *Applied Catalysis A: General*, vol. 386, no. 1-2, pp. 94–100, 2010.

[17] A. G. Abraham, A. Manikandan, E. Manikandan et al., "Enhanced magneto-optical and photo-catalytic properties of transition metal cobalt (Co^{2+} ions) doped spinel $MgFe_2O_4$ ferrite nanocomposites," *Journal of Magnetism and Magnetic Materials*, vol. 452, pp. 380–388, 2018.

[18] D. Kang, X. Yu, M. Ge, and W. Song, "One-step fabrication and characterization of hierarchical $MgFe_2O_4$ microspheres and their application for lead removal," *Microporous and Mesoporous Materials*, vol. 207, pp. 170–178, 2015.

[19] V. Srivastava, Y. C. Sharma, and M. Sillanpää, "Application of nano-magnesso ferrite (n-$MgFe_2O_4$) for the removal of Co^{2+} ions from synthetic wastewater: kinetic, equilibrium and thermodynamic studies," *Applied Surface Science*, vol. 338, pp. 42–54, 2015.

[20] M. Kaur, N. Kaur, K. Jeet, and P. Kaur, "$MgFe_2O_4$ nanoparticles loaded on activated charcoal for effective removal of Cr (VI)-a novel approach," *Ceramics International*, vol. 41, no. 10, pp. 13739–13750, 2015.

[21] N. Sivakumar, S. R. P. Gnanakan, K. Karthikeyan et al., "Nanostructured $MgFe_2O_4$ as anode materials for lithium-ion batteries," *Journal of Alloys and Compounds*, vol. 509, no. 25, pp. 7038–7041, 2011.

[22] S. Kanagesan, M. Hashim, S. Tamilselvan, N. B. Alitheen, I. Ismail, and G. Bahmanrokh, "Cytotoxic effect of nanocrystalline $MgFe_2O_4$ particles for cancer cure," *Journal of Nanomaterials*, vol. 2013, Article ID 865024, 8 pages, 2013.

[23] J. Patil, D. Nadargi, I. S. Mulla, and S. S. Suryavanshi, "Spinel $MgFe_2O_4$ thick films: a colloidal approach for developing gas sensors," *Materials Letters*, vol. 213, pp. 27–30, 2018.

[24] Y. Zu, Y. Zhao, K. Xu, Y. Tong, and F. Zhao, "Preparation and comparison of catalytic performance for nano $MgFe_2O_4$, GO-loaded $MgFe_2O_4$ and GO-coated $MgFe_2O_4$ nanocomposites," *Ceramics International*, vol. 42, no. 16, pp. 18844–18850, 2016.

[25] M. M. Rashad, "Magnetic properties of nanocrystalline magnesium ferrite by co-precipitation assisted with ultrasound irradiation," *Journal of Materials Science*, vol. 42, no. 13, pp. 5248–5255, 2007.

[26] S. Ilhan, S. G. Izotova, and A. A. Komlev, "Synthesis and characterization of $MgFe_2O_4$ nanoparticles prepared by hydrothermal decomposition of co-precipitated magnesium and iron hydroxides," *Ceramics International*, vol. 41, no. 1, pp. 577–585, 2014.

[27] S. Akbari, S. M. Masoudpanah, S. M. Mirkazemi, and N. Aliyan, "PVA assisted coprecipitation synthesis and characterization of $MgFe_2O_4$ nanoparticles," *Ceramics International*, vol. 43, no. 8, pp. 6263–6267, 2017.

[28] S. Reddy, B. E. Kumara Swamy, U. Chandra, K. R. Mahathesha, T. V. Sathisha, and H. Jayadevappa, "Synthesis of $MgFe_2O_4$ nanoparticles and $MgFe_2O_4$ nanoparticles/CPE for electrochemical investigation of dopamine," *Analytical Methods*, vol. 3, no. 12, pp. 2792–2796, 2011.

[29] A. Pradeep, P. Priyadharsini, and G. Chandrasekaran, "Sol-gel route of synthesis of nanoparticles of $MgFe_2O_4$ and XRD, FTIR and VSM study," *Journal of Magnetism and Magnetic Materials*, vol. 320, no. 21, pp. 2774–2779, 2008.

[30] M. Goodarz Naseri, M. H. M. Ara, E. B. Saion, and A. H. Shaari, "Superparamagnetic magnesium ferrite nanoparticles fabricated by a simple, thermal-treatment method," *Journal of Magnetism and Magnetic Materials*, vol. 350, pp. 141–147, 2014.

[31] Y. Feng, S. Li, Y. Zheng, Z. Yi, Y. He, and Y. Xu, "Preparation and characterization of $MgFe_2O_4$ nanocrystallites via PVA sol-gel route," *Journal of Alloys and Compounds*, vol. 699, pp. 521–525, 2017.

[32] T. Sasaki, S. Ohara, T. Naka et al., "Continuous synthesis of fine $MgFe_2O_4$ nanoparticles by supercritical hydrothermal reaction," *Journal of Supercritical Fluids*, vol. 53, no. 1–3, pp. 92–94, 2010.

[33] B. S. Randhawa, H. Kaur, H. S. Dosanjh, and J. Singh, "Precursor route for the synthesis of $MgFe_2O_4$ nanoparticles from the thermolysis of magnesium hexapropionatoferrate(III)," *Ceramics International*, vol. 42, no. 7, pp. 8891–8894, 2016.

[34] Y. Shen, Y. Wu, X. Li, Q. Zhao, and Y. Hou, "One-pot synthesis of $MgFe_2O_4$ nanospheres by solvothermal method," *Materials Letters*, vol. 96, pp. 85–88, 2013.

[35] T. Lazarova, M. Georgieva, D. Tzankov et al., "Influence of the type of fuel used for the solution combustion synthesis on the structure, morphology and magnetic properties of nanosized

$NiFe_2O_4$," *Journal of Alloys and Compounds*, vol. 700, pp. 272–283, 2017.

[36] M. M. Rashad, M. G. El-Shaarawy, N. M. Shash, M. H. Maklad, and F. A. Afifi, "Controlling the composition, microstructure, electrical and magnetic properties of $LiFe_5O_8$ powders synthesized by sol gel auto-combustion method using urea as a fuel," *Journal of Magnetism and Magnetic Materials*, vol. 374, pp. 495–501, 2015.

[37] R. Sen, P. Jain, R. Patidar, S. Srivastava, R. S. Rana, and N. Gupta, "Synthesis and characterization of nickel ferrite ($NiFe_2O_4$) nanoparticles prepared by sol-gel method," *Materials Today: Proceedings*, vol. 2, no. 4-5, pp. 3750–3757, 2015.

[38] K. C. Patil, M. S. Hegde, T. Rattan, and S. T. Aruna, *Chemistry of Nanocrystalline Oxide Materials: Combustion Synthesis, Properties and Applications*, World Scientific, Singapore, 2008.

[39] P. Lee, E. Saion, N. Al-Hada, and N. Soltani, "A simple up-scalable thermal treatment method for synthesis of ZnO nanoparticles," *Metals*, vol. 5, no. 4, pp. 2383–2392, 2015.

[40] R. Lamba, A. Umar, S. K. Mehta, and S. K. Kansal, "CeO_2ZnO hexagonal nanodisks: efficient material for the degradation of direct blue 15 dye and its simulated dye bath effluent under solar light," *Journal of Alloys and Compounds*, vol. 620, pp. 67–73, 2015.

[41] P. Annie Vinosha, B. Xavier, A. Ashwini, L. Ansel Mely, and S. Jerome Das, "Tailoring the photo-Fenton activity of nickel ferrite nanoparticles synthesized by low-temperature coprecipitation technique," *Optik*, vol. 137, pp. 244–253, 2017.

[42] M. M. Rashad, R. M. Mohamed, M. A. Ibrahim, L. F. M. Ismail, and E. A. Abdel-Aal, "Magnetic and catalytic properties of cubic copper ferrite nanopowders synthesized from secondary resources," *Advanced Powder Technology*, vol. 23, no. 3, pp. 315–323, 2012.

[43] F. A. Harraz, R. M. Mohamed, M. M. Rashad, Y. C. Wang, and W. Sigmund, "Magnetic nanocomposite based on titania-silica/cobalt ferrite for photocatalytic degradation of methylene blue dye," *Ceramics International*, vol. 40, no. 1, pp. 375–384, 2014.

[44] N. G. Yadav, L. S. Chaudhary, P. A. Sakhare, T. D. Dongale, P. S. Patil, and A. D. Sheikh, "Impact of collected sunlight on $ZnFe_2O_4$ nanoparticles for photocatalytic application," *Journal of Colloid and Interface Science*, vol. 527, pp. 289–297, 2018.

[45] A. Kalam, A. G. Al-Sehemi, M. Assiri et al., "Modified solvothermal synthesis of cobalt ferrite ($CoFe_2O_4$) magnetic nanoparticles photocatalysts for degradation of methylene blue with H_2O_2/visible light," *Results in Physics*, vol. 8, pp. 1046–1053, 2018.